Low dose positron emission tomography emulation from decimated high statistics: A clinical validation study

Josh Schaefferkoetter[a)]
*A*STAR-NUS, Clinical Imaging Research Centre, Singapore, Singapore*
Joint Department of Medical Imaging, University Health Network, Toronto, ON, Canada
Siemens Healthcare Limited, Oakville, ON, Canada

Ying-Hwey Nai, Anthonin Reilhac, and David William Townsend
*A*STAR-NUS, Clinical Imaging Research Centre, Singapore, Singapore*

Lars Eriksson and Maurizio Conti
Siemens Medical Solutions USA, Inc., Knoxville, TN, USA

(Received 15 January 2019; revised 1 March 2019; accepted for publication 21 March 2019; published 3 May 2019)

Purpose: The fundamental nature of positron emission tomography (PET), as an event detection system, provides some flexibility for data handling, including retrospective data manipulation. The reorganization of acquisition data allows the emulation of new scans arising from identical radiotracer spatial distributions, but with different statistical compositions, and is especially useful for evaluating the stability and reproducibility of reconstruction algorithms or when investigating extremely low count conditions. This approach is ubiquitous in the research literature but has only been validated, from the point of view of the noise properties, with numerical simulations and phantom data. We present here the first experiment comparing PET images of the same human subjects generated with two separate injections of radiotracer, using actual low dose (LD) data to validate a randomly decimated emulation from a standard dose scan. A key point of the work is focused on the randoms fractions, which scale differently than the trues at varying activity levels.
Methods: Eleven patients with non-small cell lung cancer were enrolled in the study. Each imaging session consisted of two independent FDG-PET/CT scans: a LD scan followed by a standard dose (SD) scan. Images were first reconstructed, using filtered back-projection (FBP) and OSEM incorporating time-of-flight information and point-spread function modeling (PSFTOF), from the LD and SD datasets comprising all counts from each scanned bed position. The number of true counts was recorded for all LD scans, and independent, count-matched emulations (ELD) were reconstructed from the SD data. Noise distribution within the liver and standardized uptake value reproducibility within a population of contoured, tracer-avid lesion volumes were evaluated across scans and statistics.
Results: The randoms fraction estimates were 17.4 $\pm$ 1.6% (14.9-19.4) in the LD data and 42 $\pm$ 2.3% (37.1-45.5) in the SD data. Eleven lesions were identified and volumes of interest were generated with a 50% threshold isocontour for each lesion, in every image. The distributions of metabolic volumes, means and maxima defined by the contoured volumes-of-interest (VOIs) were similar between the LD and SD sets. A two-tailed, matched t-test was performed on the populations of region statistics for both LD and ELD reconstructions, and the t-statistics were 1.1 (P = 0.267) and -0.22 (P = 0.828) for the background liver VOIs and -0.54 (P = 0.603) and 0.23 (P = 0.821) for the lesion VOIs, for FBP and PSFTOF respectively. In every test, the null hypothesis that the two populations had the same mean could not be rejected at the 5% significance level.
Conclusions: Our results demonstrate that clinical LD PET scans can indeed be accurately emulated by the statistical decimation of standard dose scans, and this was achieved through validation by images generated with unbiased random coincidence estimations. [https://doi.org/10.1002/mp.13517]

Key words: emulation, listmode, low dose PET

1. INTRODUCTION

Positron emission tomography (PET) is a valuable diagnostic tool for a growing number of pathological indications. Its clinical adoption has been facilitated by significant advances in hardware and software technology and is predicated on continual, rigorous assessment of scanner performance by the research community. Image quality, with contrast and noise

as the general metrics of interest, is typically evaluated through computational simulations,[1,2] phantom scans[3,4] or investigations using actual human subject data,[5,6] with the last approach often being viewed as the most relevant to the medical setting.

The fundamental nature of PET, as an event detection system, provides some flexibility for data handling, including retrospective data manipulation. In particular, when the stream of acquisition events is collected and stored in listmode format, the data can be selectively reorganized. This technique allows the emulation of new scans arising from identical radiotracer spatial distributions, but with different statistical compositions (i.e., the number of counts available for image reconstruction); it is especially useful for evaluating the stability and reproducibility of reconstruction algorithms or when investigating extremely low count conditions.[7,8] Different approaches have been proposed for creating emulated realizations, like parametric and non-parametric bootstrapping[9–11] and fully independent data realizations.[12] These methods have been validated and compared, in particular from the point of view of the noise properties, with phantom data, but not with data from patient scans. This is an important consideration since analyses of tracer distribution may be more problematic in complex, physiological systems. Furthermore, the emulation process may also be complicated by biological uptake which changes in time.

It is particularly interesting to assess image quality, noise, and texture characteristics of low dose (LD) PET patient scans. In the past, we evaluated image quality in very low count data via decimating a standard dose in real patient scans, for the purpose of evaluating PET/CT screening.[7,8] Based on these previous studies, a very LD protocol has been devised, and a new study is ongoing which compares the LD PET/CT images with the standard PET/CT images on the same patients, receiving these two independent PET/CT scans on the same day.[13] Using the patient data of this study, we focused on the validation of the decimation method. This application adds a further complexity because of the different random fraction at low and standard dose — that is, the true coincidence data scale linearly with the in-field activity whereas the randoms follow a quadratic curve. Generally speaking, the random data must be estimated and handled differently than the prompt measurement, and in this paper, we are addressing the case when one would like to emulate LD scans using listmode data which have inherently higher random fractions.

We present here the first experiment, to our knowledge, comparing PET images of the same human subjects generated with two separate injections of radiotracer, using actual LD data to validate a randomly decimated emulation from a standard dose scan. The subjects underwent two independent scanning sessions on the same day, while in the same physiological state, but with different radiotracer doses. The standard dose scan was *a posteriori* decimated in order to emulate the same count statistics of the LD scan. We report acquisition properties and reconstructed noise characteristics at different statistical levels for various anatomical regions, as well as compare the images generated using emulated reduced-count PET data to those of the actual LD scans. A key issue, often overlooked in LD simulations, is the difference in random fraction between a randomly decimated standard dose scan and an actual LD scan — this topic is discussed in this work.

The purpose of this work is to assess whether LD PET scans can be accurately emulated by the decimation of standard dose scans. It was motivated by the lack of validation

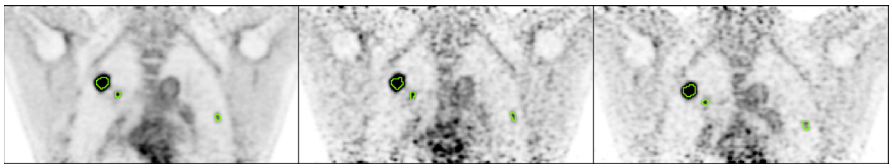

FIG. 1. Coronal slices showing volumes-of-interest (VOIs) drawn over lung lesions for standard dose (SD) (left), emulated low dose (center), and low dose (right) images. In every case, the VOIs comprising the top 50% of the voxels defined the mask, creating unique lesion segmentations for each image. The images seen here were reconstructed with point-spread function modeling. [Color figure can be viewed at wileyonlinelibrary.com]

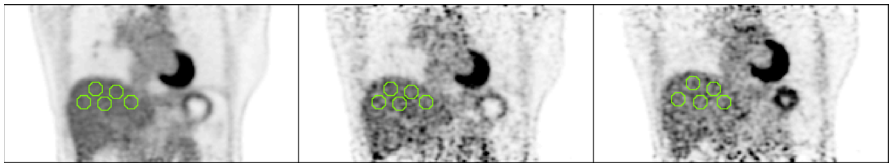

FIG. 2. Coronal slices showing spherical volumes-of-interest (VOIs) drawn in the liver for standard dose (SD) (left), emulated low dose (ELD) (center), and low dose (right) images — the SD and ELD images, are realized from the same dataset and hence share the same VOIs. These images were reconstructed with point-spread function modeling. [Color figure can be viewed at wileyonlinelibrary.com]

data within a population of human subject datasets, making it difficult to understand and characterize any potential differences within a clinical context. The findings presented here could be especially relevant to studies investigating clinical scanner performance limits and LD patient imaging. We focus solely on the decimation method which generates fully independent realizations, as this is the most realistic surrogate for real LD data.

2. MATERIALS AND METHODS

2.A. Patient population and data acquisition

Eleven patients with non-small cell lung cancer consented and were enrolled in the study. Each imaging session consisted of two fluorodeoxyglucose (FDG)-PET/CT scans on a Biograph mCT (Siemens Healthcare Molecular Imaging): a LD scan followed by a standard dose (SD) scan.

For the LD scan, subjects were given a LD injection of 26.6 ± 3.7 (19.2–30.7) MBq. After a 60-min uptake, they were instructed to void the bladder, after which they were positioned on the scanning bed. They were scanned in 1 or 2 bed positions over the thorax and abdomen for 10 min per bed — the LD CT parameters were 120 kVp, 40 mAs (careDose), pitch 1. After completion of the LD PET/CT scan, the patient was moved back into the uptake room to rest for 30 minutes before given another FDG injection, this time a standard dose of 225.3 ± 5.6 (214.6–233.1) MBq. There was another 60-min uptake period and bladder voiding before being moved back onto the scanning bed for a SD PET/CT. The patient was scanned with the same thoracic coverage and duration as the LD scan, however, the CT parameters were 120 kVp, 140 mAs (careDose), pitch 1.5.

For the SD scan, we assumed the contribution from the first LD FDG injection was negligible since, at the second scan time, it accounted for around 4% of the total activity in the patient. This number is below the standard accepted test-retest variability of current PET technology.[6,14]

2.B. Image processing and analysis

Nine subjects were scanned with two bed positions and two subjects were scanned with 1 bed position, yielding a total of 20 beds, individually covering the same anatomic regions in each of the LD and SD sessions. The PET acquisition data were reconstructed independently per bed, that is, patient "whole-body" volumes were not generated.

Images were first reconstructed from the LD and SD datasets comprising all counts from each scanned bed position. Then, the numbers of true counts (prompt — random events) were recorded, per bed, for all LD scans. The SD data were decimated to match the corresponding LD true count level — the events contained in the SD listmodes were randomly sorted into bins and stored in smaller, emulated low dose (ELD) listmode files. Each dataset was independent, that is, there were no shared events among the realizations, and the maximum number of independent ELD listmode files was generated for each paired dataset.

The term "true counts", as it is used throughout this paper, actually include the scatter events as well, but for the matched LD and ELD data, the actual true coincidence levels are equivalent since the scatter fractions are essentially identical. Theoretically, PET images reconstructed from the same number of true counts should share the same image properties, and hence, it is reasonable to expect that emulated scans would be equivalent to real scans acquired at the same count level. However, although the net trues rate scales linearly with the in-field activity, the randoms rate scales by the square of the singles. This means that prompt acquisition measurements are affected by both of these phenomena and the ELD data have randoms fractions equivalent to their standard dose counterpart. The higher randoms fractions do result in a lower noise equivalent count rate for the ELD data, and the efficacy of the randoms correction, which in this study was based on a smoothed measurement of the delayed coincidence events,[15] is a key focus of the work.

The low dose PET data were acquired alongside a corresponding low dose CT protocol. It has been previously demonstrated that accuracy of the CT-derived attenuation correction is not degraded even at ultra-low CT levels.[16] Hence, the CT images were used for attenuation and scatter corrections without considering differences between the CT acquisitions on the PET quantification.

All original and emulated listmode data were reconstructed separately using two reconstruction algorithms: filtered back-projection (FBP) and ordered subset expectation maximization, incorporating time-of-flight information and point-spread function modeling (PSFTOF). The reconstructed image matrix was 400 × 400 × 109 with voxel dimensions 2.0364 × 2.0364 × 2.027 mm — a post-reconstruction 3 mm FWHM Gaussian smoothing filter was applied. The PSFTOF reconstructions used two iterations and 21 subsets.

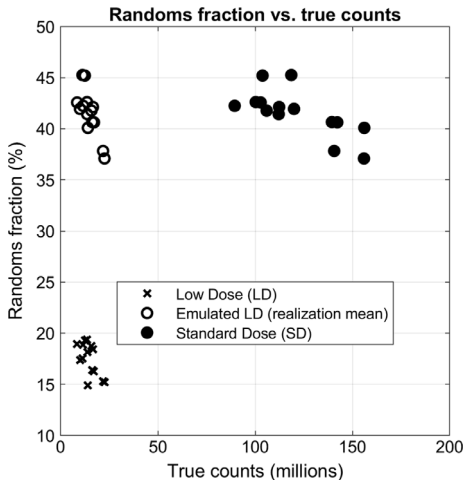

FIG. 3. Randoms fractions as a function of net true counts. Emulated low dose data, matched to the net true level of a real low dose set, still retain the original randoms fraction of their standard dose parents.

Image analysis was performed using volumes-of-interest (VOIs) drawn over cancer lesions in the lungs and over uniform background regions in the liver, matched in both PET acquisitions. Eleven VOIs were drawn over lung lesions in eight beds using a 50% isocontour, independently within each PET image; one patient containing two lesions is shown in Fig. 1. The stability of contoured metabolic volumes and standardized uptake value (SUV) measurements across scans and statistics were studied in these lesions VOIs.

The noise texture in the liver was used as a surrogate of overall image noise. For eight bed positions containing the subjects' abdomens, non-overlapping spherical VOIs, each comprising 515 voxels (~4.33 cm^3), were drawn within the liver for the SD, ELD, and LD images, as seen in Fig. 2. To avoid excessive contamination from high-frequency noise at the edges of the axial field-of-view (FOV), the VOIs were restricted to lie within the center 50% of the FOV.

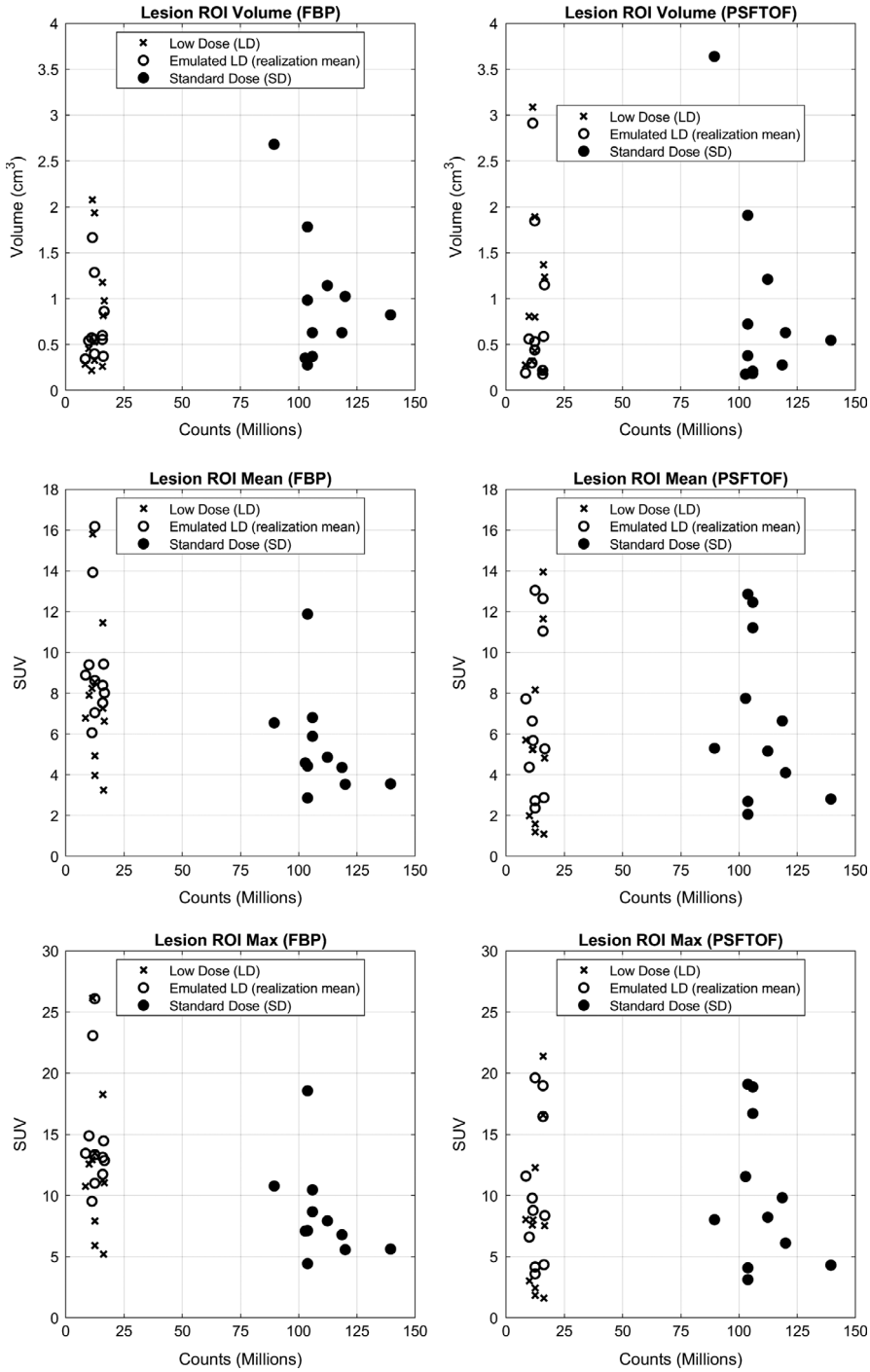

FIG. 4. Lesion VOI volume, mean and max standardized uptake value data, shown for 11 lesions.

Physiological motion was also a consideration during the VOI selection process. Attenuation-activity mismatches due to respiration affect the PET attenuation correction and cause image artifacts which deteriorate local image quantification, especially at regions located adjacent to the inferior lung boundary near the diaphragm. Additionally, since the CT data might be acquired at different respiratory phases, the degree of mismatch between two independent scans may be inconsistent. Considering this, the liver VOIs, as well as the lung lesion VOIs, were carefully compared between the SD and LD data in order to avoid any relative bias due to attenuation map misregistration.

For each spherical liver VOIs, the coefficient of variation (CV), that is, the standard deviation among the voxels within the VOI as a percentage of the corresponding mean, was recorded as the metric of interest. This was only measured once for the LD images, but for the multiple realizations of the ELD images, the mean CV across realizations was stored for each VOI. A paired t-test was performed to determine if the LD and ELD statistics had the same distribution. All the VOI statistics from the LD images were pooled into one population, and those from the ELD images pooled into another. A two-tailed test was performed within the liver VOIs on the matched LD and ELD populations against the null hypothesis that the populations had the same mean.

3. RESULTS

The mean true count rates for the SD and LD scans were 132.7 ± 57.6 and 16.4 ± 7.2 million per bed position, respectively, and the number of independent realizations per bed was 8 (6–12). The detection rates of random coincident

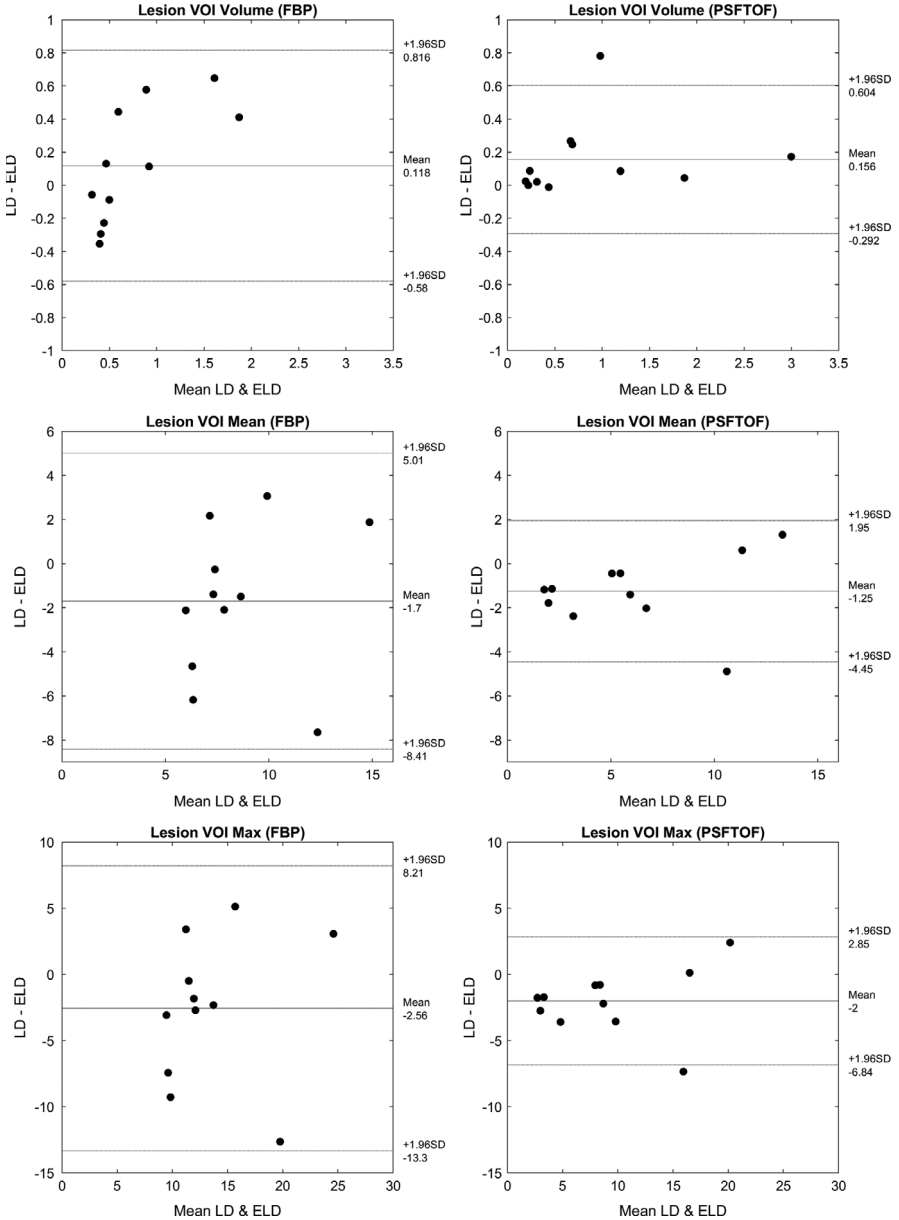

FIG. 5. Bland-Altman plots representing the low dose and emulated low dose lesion metrics shown in Fig. 4.

events do not scale linearly with the true counts, and the estimated randoms fractions were much larger in the SD scans. As seen in Fig. 3, in this study, the randoms rates were 17.4 ± 1.6% (14.9–19.4) for LD and 42 ± 2.3% (37.1–45.5) for SD.

Eleven lesions were identified and VOIs were generated with a 50% threshold isocontour — this was repeated for each lesion, in every image. The average volumes defined by the contoured VOIs were 0.8 ± 0.66 cm^3, 0.7 ± 0.42 cm^3 and 1.0 ± 0.71 cm^3, as measured in the FBP images, and 1.0 ± 0.90 cm^3, 0.8 ± 0.86 cm^3 and 0.9 ± 1.05 cm^3, in the PSFTOF images, for the LD, ELD and SD datasets, respectively. The distributions of lesion VOI volumes, along with the corresponding SUV means and maxes, are seen in Fig. 4. For clarity, Bland-Altman plots comparing the LD and ELD measurements are shown in Fig. 5, and a breakdown of the lesion metrics is given in Table I.

The correlations between lesion mean and max SUVs measured in the SD and ELD images were also investigated. As seen in Fig. 6, excellent SUV correlation was observed within images reconstructed with PSFTOF. The correlation in the FBP reconstructions was poorer, which was due to image noise and increased measurement values of max lesion SUV. This affected the VOI boundary threshold — in general, region volume decreased while mean SUV increased. For the ELD data, the realization mean is plotted and the error bars denote the measurement standard deviation across the realizations.

Out of the 20 total beds, eight were found to have sufficient coverage over the liver, within the center of the FOV, in both the SD and LD images. In total, 64 liver VOIs were drawn in each image set — the mean number of liver VOIs per bed was 8 ± 2.6. The VOI CV, as a function of net true level, is shown in Fig. 7, along with the corresponding Bland-Altman plots comparing the background measurements in the LD and ELD images.

It can also be seen from the data in Fig. 7 that the CV in the background regions, as a surrogate for overall image noise, generally follows the inverse square root of the true counts. Within the identical regions in the ELD and SD data, the linear correlations between the noise ratios and the inverse square roots of the count ratios yielded R^2 values 0.96 and 0.87 for the FBP and PSFTOF images, respectively.

A 2-tailed, matched t-test was used to test the null hypothesis that the populations of LD and ELD statistics had the same distributions. The test was performed for both reconstructions, and the t-statistics were 1.1 (P = 0.267) and −0.22 (P = 0.828) for the background liver VOIs and −0.54 (P = 0.603) and 0.23 (P = 0.821) for the lesion VOIs, for FBP and PSFTOF, respectively. Additionally, the tests were performed on the matched statistics within each bed independently. In every test, the null hypothesis that the two populations had the same mean could not be rejected at the 5% significance level.

4. DISCUSSION

The statistical decimation of a large PET dataset provides a simple yet powerful method for emulating low count PET

TABLE I. Breakdown of the metrics of the 11 lesions shown in Fig. 4.

	VOI Volume (cm^3)						VOI Mean (SUV)						VOI Max (SUV)					
	FBP			PSFTOF			FBP			PSFTOF			FBP			PSFTOF		
Lesion	LD	ELD	SD	LD	ELD	SD	LD	ELD	SD	LD	ELD	SD	LD	ELD	SD	LD	ELD	SD
1	2.08	1.67 ± 1.11	2.68	3.09	2.91 ± 0.54	3.64	15.80	13.92 ± 1.37	6.54	5.24	5.68 ± 0.35	5.30	26.13	23.06 ± 1.85	10.78	7.99	8.77 ± 0.70	8.02
2	0.22	0.57 ± 0.19	0.63	0.32	0.30 ± 0.08	0.28	8.23	6.06 ± 0.65	4.36	5.23	6.63 ± 0.60	6.64	12.94	9.53 ± 1.01	6.79	7.58	9.79 ± 0.83	9.82
3	0.82	0.37 ± 0.15	0.82	1.37	0.59 ± 0.25	0.55	3.25	9.42 ± 1.62	3.55	1.09	2.87 ± 0.34	2.81	5.20	14.46 ± 2.36	5.62	1.61	4.35 ± 0.51	4.31
4	1.93	1.29 ± 0.24	1.78	1.89	1.85 ± 0.17	1.91	8.53	16.17 ± 1.10	11.88	8.16	13.04 ± 0.59	12.86	13.45	26.08 ± 2.07	18.56	12.27	19.61 ± 1.08	19.08
5	0.53	0.40 ± 0.10	0.28	0.43	0.44 ± 0.17	0.38	3.97	8.62 ± 0.74	4.43	1.58	2.72 ± 0.42	2.69	5.90	13.33 ± 1.11	7.13	2.44	4.16 ± 0.61	4.08
6	0.33	0.56 ± 0.13	0.98	0.80	0.53 ± 0.16	0.72	4.92	7.04 ± 0.50	2.86	1.19	2.36 ± 0.30	2.06	7.93	11.00 ± 0.95	4.43	1.83	3.59 ± 0.43	3.13
7	1.18	0.60 ± 0.17	0.63	0.22	0.22 ± 0.03	0.21	7.26	7.52 ± 0.75	5.88	11.65	11.04 ± 0.70	11.21	11.24	11.73 ± 1.46	8.67	16.58	16.45 ± 1.03	16.70
8	0.26	0.55 ± 0.29	0.37	0.20	0.18 ± 0.01	0.18	11.45	8.38 ± 1.57	6.80	13.95	12.64 ± 0.65	12.46	18.25	13.12 ± 2.28	10.46	21.38	18.97 ± 1.23	18.87
9	0.45	0.54 ± 0.25	1.03	0.81	0.56 ± 0.10	0.63	7.90	9.39 ± 1.16	3.53	1.99	4.37 ± 0.39	4.10	12.57	14.88 ± 2.12	5.57	3.01	6.60 ± 0.57	6.11
10	0.29	0.34 ± 0.13	0.35	0.28	0.19 ± 0.02	0.18	6.79	8.88 ± 1.38	4.58	5.70	7.72 ± 0.83	7.75	10.74	13.44 ± 2.09	7.09	8.03	11.58 ± 1.31	11.55
11	0.98	0.86 ± 0.41	1.14	1.24	1.15 ± 0.28	1.21	6.62	8.01 ± 1.86	4.86	4.82	5.27 ± 0.35	5.16	11.04	12.86 ± 2.46	7.92	7.54	8.36 ± 0.66	8.22

VOI, volumes-of-interest; SUV, standardized uptake value; FBP, filtered back-projection; PSFTOF, point-spread function modeling; LD, low dose; ELD, emulated low dose; SD, standard dose.

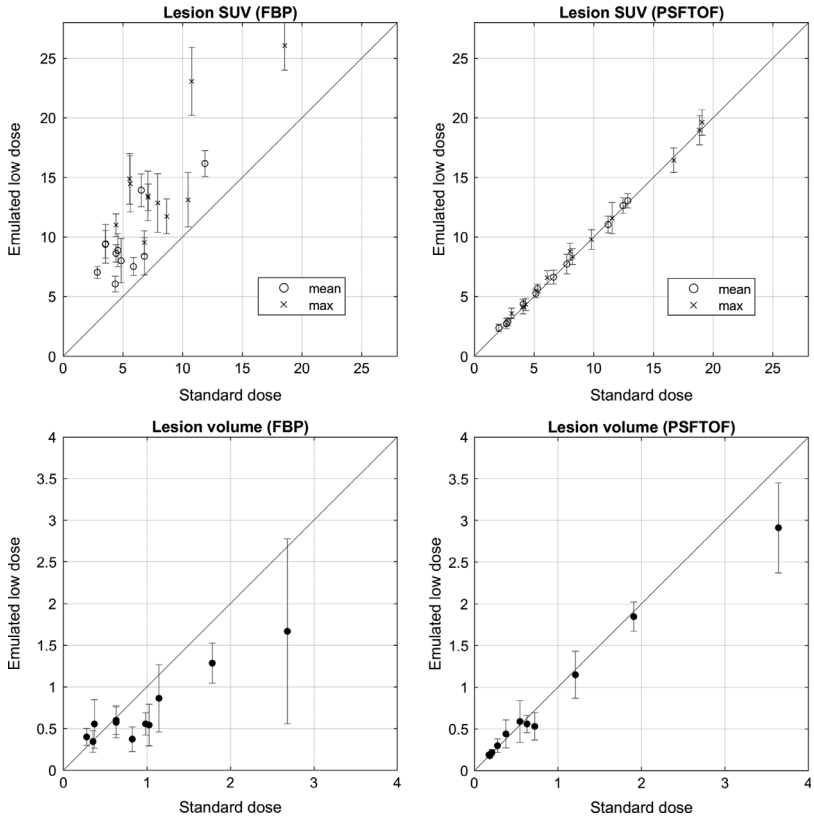

FIG. 6. Correlations between standard dose and emulated low dose measurements of mean and max standardized uptake value and volume for all lesion volumes-of-interests.

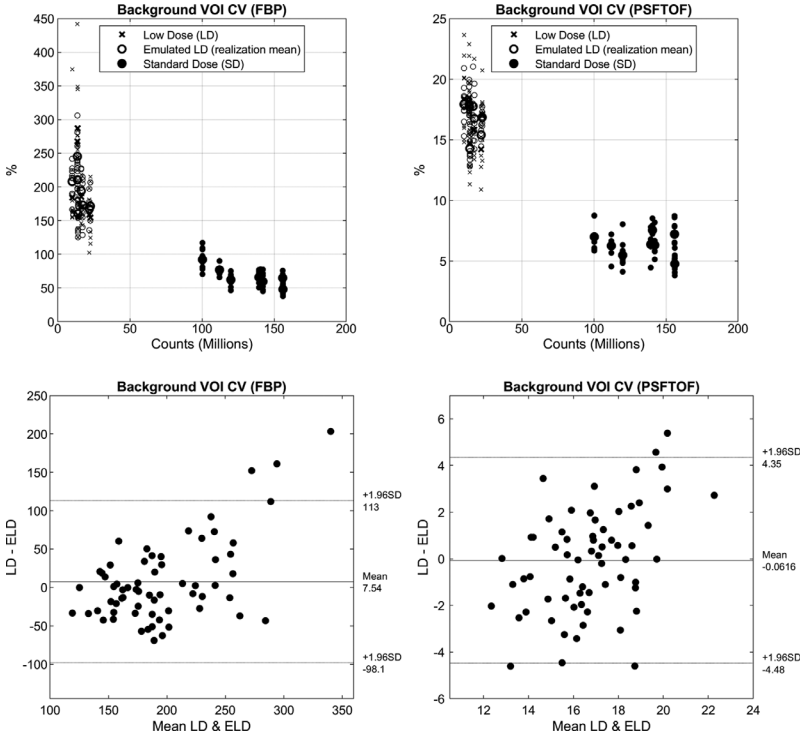

FIG. 7. In the top two plots, the coefficient of variation (CV) as a function of net true count level is shown for background volumes-of-interests (VOIs) drawn in the liver. The CV of each VOI is represented by the faint markers, the mean over all VOIs for a given bed position are shown in bold. The bottom two Bland-Altman plots compare the corresponding the low dose and emulated low dose metrics. Note the different axes scales between the two reconstructions needed to represent the data.

images and generating different realizations of a given activity distribution. The validity of this approach as a surrogate for real low count conditions has been demonstrated in numerical simulations and phantom scans but never in a cohort of human subjects — this was the motivation for the work here. This study was designed specifically to compare real PET images corresponding to different radiotracer doses in the same subject, ensuring that the physiological state of each subject was constant between scans.

Although different inherent randoms fractions could potentially lead to differences between the real and emulated data, the results presented here showed that the correction was robust and compensated for different randoms fractions. The data in Fig. 4 show that there were no significant measured differences, between LD and ELD images, in the standard metrics used to quantify regions of focal uptake. There was also no relative bias observed in the reconstructed data in regards to image noise or SUV, as seen in Fig. 7 and confirmed statistically by the paired t-tests. The correction used throughout this study involved a randoms estimation based on a smoothed measurement of the delayed coincidence events. A subset of the data was processed independently without randoms smoothing and analyzed, yielding similar results — though the effects may be larger for very noisy delayed coincidence acquisitions.

The scatter correction has been shown to pose a problem for extremely low dose PET, specifically because the noisy tails in the emission projections yield unreliable scaling of the scatter contribution, usually overestimating its amplitude.[8] This, however, was not a point of interest in this study because the scatter estimation behaves similarly between LD and ELD data. Furthermore, the count levels included in this work were much higher than the extreme low cases reported to be problematic.

We note that the results presented in this work are applicable to PET data with the signal and noise levels characteristic of standard and low dose FDG studies. Different findings might be expected with data having higher overall count rates or those involving prompt gamma-emitting tracers, for example, Rubidium-82.

5. CONCLUSION

This work investigated the validity of listmode decimation for generating clinical PET images of reduced statistics. The extraction of independent and random subsets from larger PET datasets was demonstrated to be a quantitatively accurate technique for emulating low-count scans as shown comparing emulated LD data with actual LD data.

[a)]Author to whom correspondence should be addressed. Electronic mail: Josh.Schaefferkoetter@uhn.ca.

REFERENCES

1. Barrett HH, Wilson DW, Tsui BM. Noise properties of the EM algorithm. I. Theory. *Phys Med Biol* 1994;39:833.
2. Jan S, Santin G, Strul D, et al. GATE: a simulation toolkit for PET and SPECT. *Phys Med Biol*. 2004;49:4543.
3. Strother S, Casey M, Hoffman E. Measuring PET scanner sensitivity: relating countrates to image signal-to-noise ratios using noise equivalents counts. *IEEE Trans Nucl Sci*. 1990;37:783–788.
4. Daube-Witherspoon ME, Karp JS, Casey ME, et al. PET performance measurements using the NEMA NU 2-2001 standard. *J Nucl Med*. 2002;43:1398–1409.
5. Halpern BS, Dahlborm M, Quon A, et al. Impact of patient weight and emission scan duration on PET/CT image quality and lesion detectability. *J Nucl Med*. 2004;45:797–801.
6. Boellaard R. Standards for PET image acquisition and quantitative data analysis. *J Nucl Med*. 2009;50(Suppl 1):11S–20S.
7. Schaefferkoetter JD, Yan J, Townsend DW, Conti M. Initial assessment of image quality for low-dose PET: evaluation of lesion detectability. *Phys Med Biol*. 2015;60:5543.
8. Schaefferkoetter JD, Yan J, Sjöholm T, Townsend DW. Quantitative accuracy and lesion detectability of low-dose FDG-PET for lung cancer screening. *J Nucl Med*. 2017;28:399–405.
9. Dahlbom M. Estimation of image noise in PET using the bootstrap method. in Nuclear Science Symposium Conference Record, 2001 IEEE. 2001. IEEE.
10. Buvat I. A non-parametric bootstrap approach for analysing the statistical properties of SPECT and PET images. *Phys Med Biol*. 2002;47:1761.
11. Lartizien C, Aubin J-B, Buvat I. Comparison of bootstrap resampling methods for 3-D PET imaging. *IEEE Trans Med Imaging*. 2010;29:1442–1454.
12. Markiewicz P, Reader A, Matthews J. Assessment of bootstrap resampling performance for PET data. *Phys Med Biol*. 2014;60:279.
13. Schaefferkoetter J, Reilhac C, Townsend D, Conti M, Tham I. An investigation of a protocol for PET/CT screening of patients at risk of lung cancer. *J Nucl Med*. 2018;59(Suppl. 1):1354.
14. Bremmer JP, van Berckel BNM, Persoon S, et al. Day-to-day test–retest variability of CBF, CMRO 2, and OEF measurements using dynamic 15 O PET studies. *Mol Imag Biol*. 2011;13:759–768.
15. Brasse D, Kinahan PE, Lartizien C, et al. Correction methods for random coincidences in fully 3D whole-body PET: impact on data and image quality. *J Nucl Med*. 2005;46:859–867.
16. Sjoholm T, Schaefferkoetter J, Townsend D. Ultralow dose CT attenuation correction for lung cancer PET/CT screening-a phantom evaluation study. *J Nucl Med*. 2016;57(Suppl. 2):308.